Significant shortening by pressure solution creep in the Dwyka diamictite, Cape Fold Belt, South Africa

Åke Fagereng

Department of Geological Sciences, University of Cape Town, Rondebosch 7701, South Africa

Corresponding author: e-mail: ake.fagereng@uct.ac.za

Abstract

The Dwyka diamictite preserves a record of horizontal shortening related to the development of the Cape Fold Belt at subgreenschist conditions. This shortening was accommodated by folding and thrust faulting, but pressure solution may also have contributed significantly to bulk deformation. Cleavage within the Dwyka group is, in the studied part of the Karoo Basin, subvertical to moderately south dipping, and approximately axial planar to regional folds. The cleavage is anastomosing, leading to the development of ‘tombstone cleavage’, and defined microscopically by thin seams of fine grained dark material. X-ray diffraction analyses show that the diamictite matrix is made up of quartz, feldspars, muscovite and chlorite. Element maps further indicate that the cleavage is defined predominantly by phyllosilicates and minor oxides, implying that it is made up of relatively insoluble material and hydrothermal alteration products. Overall, the cleavage therefore formed by dissolution and removal of mobile elements. This indicates that pressure solution likely accommodated a significant component of shortening during the Cape Orogeny, and provides an example of low temperature cleavage development during orogenesis.

Introduction

On short time scales, the upper crust deforms by high strain rate brittle deformation (Byerlee, 1978, Sibson, 1983; Kohlstedt et al., 1995); whereas on longer time scales, the upper crust can deform ductilely at slower strain rates by viscous deformation controlled by stress-driven, fluid-assisted, diffusive mass transfer (Durney, 1972; McClay, 1977; Rutter, 1983; Gratier et al., 2013). These deformation styles may coexist spatially, as illustrated by coeval folds and faults in foreland fold-and-thrust belts (e.g. Suppe, 1983; Mitra, 1990; Mantero et al., 2011). During such coeval brittle-viscous deformation, brittle deformation is envisaged to occur episodically at fast strain rates, between longer episodes dominated by continuous viscous deformation (e.g. Gratier and Gamond, 1990; Gratier et al., 2013).

The Cape Fold Belt records ductile behaviour of rocks deformed in the upper crust (du Toit, 1937; de Wit and Ransome, 1992; Fagereng, 2012), and represents a natural laboratory for the contribution of pressure solution to large scale folding. The Dwyka Group diamictite, at the base of the Karoo Supergroup which fills the foreland basin of the Cape Fold Belt, has a particularly striking subvertical to steeply inclined cleavage, here argued to result from pressure solution, the dissolution of material by grain boundary, fluid-assisted, stress-driven diffusion. The purpose of this paper is to describe the spaced solution cleavage in the Dwyka Group in detail, and discuss its formation and role in the development of the Cape Fold Belt, with implications for pressure solution in fold-and-thrust belts in general.

Geological setting

The Cape Fold Belt formed along the southern margin of Gondwana (du Toit, 1937; de Wit and Ransome, 1992; Hälbich, 1992), in response to compression and accretion in a fold belt that can be traced from the Sierra de la Ventana in Argentina, through South Africa, to the Trans-Antarctic Mountains (du Toit, 1937; de Wit and Ransome, 1992; Dalziel et al., 2000). In a South African context, deformation related to this fold belt affects clastic sedimentary rocks of the Ordovician to Early Carboniferous Cape Supergroup, and the Late Carboniferous to Middle Jurassic Karoo Supergroup. The Cape Fold Belt is divided into a 'western arm', with a north-south structural trend, and a 'southern arm', where structures generally strike east-west (Figure 1a). The two arms meet northeast of Cape Town, in the syntaxis of the fold belt. The southern arm, in which the current study area is located, is characterised by north-verging folds and reverse faults recording predominantly north-south shortening (Hälbich, 1993; Paton *et al*., 2006; Lindeque *et al*., 2011)(Figure 1b). Cross-section reconstructions and field observations indicate at least two episodes of tectonic reactivation affecting rocks of the Cape and Karoo Supergroups: (1) formation of the Cape Fold Belt involved positive inversion of normal faults, developed before and during deposition of the Cape Supergroup in an intra-continental clastic margin; and (2) negative inversion of Cape Fold Belt related structures during the break-up of Gondwana (Paton *et al*., 2006).

The Cape Fold Belt is generally thought to reflect shallow angle subduction of the paleo-Pacific towards the north underneath Gondwana (Lock, 1980; de Wit and Ransome, 1992; Hälbich, 1992, 1993). Alternative tectonic models for the collision, however, include a transpressional setting (Tankard *et al*., 2009) and subduction towards the south, culminating in collision with a crustal block now part of South America (Lindeque *et al*., 2011). The Karoo Basin is considered to be a retro-arc foreland basin, which formed in response to the tectonic load caused by mountain building in the Cape Fold Belt (Catuneanu *et al*., 1998, 2005; Catuneanu, 2004). Tankard *et al*. (2009) have, however, suggested that the Cape Fold Belt initiated only in the Triassic, after the late Carboniferous initiation of sedimentation in the Karoo Basin. In their model, Karoo subsidence was facilitated by crustal-scale faults and not associated with a foreland basin. Irrespective of large-scale tectonic model, the Cape Fold Belt and Karoo Basin developed with some overlap in time, and the Karoo Basin was filled by sediments derived by erosion of the adjacent mountains of the Cape Fold Belt (e.g. Catuneanu *et al*., 2005 and references therein). The sediments of the Karoo Basin, in areas adjacent to the Cape Fold Belt, were then also deformed as a result of regional compression.

The Dwyka Group is the oldest sedimentary unit of the Karoo Supergroup, and reflects a Gondwana glaciation from 302 to 290 Ma (Bangert *et al*., 1999). The Dwyka Group is present over large areas of southern Africa, and contains both continental and marine facies (Visser, 1987, 1997; Visser *et al*., 1997). Here, focus is on deformation of the Dwyka in an area adjacent to the Cape Fold Belt, and therefore in the foredeep marine facies as discussed by Catuneanu (2004). In the foredeep of the proposed retro-arc foreland Karoo Basin, the Dwyka Group comprises four upward-fining sequences of massive to stratified diamictites reaching up to 800 m in total thickness (Visser, 1997). The diamictites are composed of a silt-dominated matrix with dropstones of variable size, shape, and composition, derived from floating ice. The strata are uniform and laterally continuous, indicating deposition from suspension in a low energy environment (Visser, 1987). In places, there is evidence for re-sedimentation by debris flow (Visser, 1997), and, in general, bedding planes are not recognizable in outcrop, because of re-sedimentation and/or bedding thicknesses exceeding the size of the outcrop.

In the study area, the Dwyka Group is separated from the underlying Cape Supergroup by an unconformity that represents approximately 30 million years of missing rock record, inferred to reflect a period of regional uplift related to collision during the mid-Carboniferous assembly of Pangea (Catuneanu *et al*., 2005). The diamictites are overlain by the Prince Albert Formation, which is the lowest part of the post-glacial Ecca Group. The transition from the Dwyka to the Ecca Group is reflected in a gradual contact between mudstones with and without dropstones respectively. The Prince Albert Formation is interpreted as a marine mudstone sequence, with sediments derived from the growing Cape Fold Belt mountains to the south (Catuneanu et al., 1998). Structure in the study area, which is in the frontal range of the Cape Fold Belt (Figure 1), represents a northward transition from north-verging, open to tight folds, to upright, open folds. Further north, the strata are approximately horizontal. Cleavage is generally axial planar, i.e. subvertical to moderately south dipping (Figure 2a,b). Horizontal pencil lineation (formed at the intersection between cleavage and bedding) attest to subhorizontal fold hinge lines. Fluid inclusions imply temperatures less than 200°C during deformation in this area (Egle *et al*., 1998).

Field and microstructural observations

In the Laingsburg region, fold geometry changes from north-verging, moderately inclined, tight to open folds with locally overturned limbs (Figures 1c, 2a), to upright, open folds (Figures 1b, 2b). The former occurs in Cape Supergroup rocks, and the Dwyka and Ecca Group rocks that crop out adjacent to the northernmost exposures of the Cape Supergroup, whereas upright folding becomes predominant further north (Figure 1b). Cleavage is generally axial planar, and as a result, cleavage in the Dwyka varies in orientation from steeply to moderately inclined, reflecting a variation in fold inclination (Figure 2c). Strike of cleavage planes, however, is relatively uniform and E-W to WNW-ESE.

At outcrop scale, cleavage in the Dwyka is anastomosing and curvi-planar. Because cleavage planes represent planes of relative weakness, mechanical erosion leads to formation of so-called ‘tombstone cleavage’, where blocks separated by anastomosing cleavage surfaces dominate the surface exposure of the Dwyka (Figure 3a,b). The long axes of these ‘tombstones’ are parallel to the average dip direction of the anastomosing cleavage planes, and therefore moderately to steeply plunging (Figure 3a,b,c). The size of the tombstones (as measured by the length of their long axes), increases as a function of the largest dropstone contained within them (Figure 4). The Dwyka diamictites also preserve fractured dropstones, where tensile fractures are constrained to the dropstones, and oriented approximately perpendicular to cleavage (Figure 3c).

At the micro-scale, the cleavage is also anastomosing and curvi-planar (Figure 5a-c). Cleavage surfaces are defined by fine-grained black material, which forms wavy surfaces through the matrix, and that wrap around dropstones and larger clasts in the matrix (Figure 5a,b). A near-perpendicular angular relationship between cleavage and tensile fractures within dropstones is apparent also on the micro-scale (Figure 5c). Because the cleavage does not cut through dropstones, but curves around them, the cleavage spacing is to a first order controlled by dropstone size (Figure 5a). On the other hand, very small spacing between cleavage surfaces occurs at the edge of some dropstones (Figure 5b). Cleavage spacing thereby varies from < 10 µm to several hundred µm. Dropstones, particularly those composed of quartz, commonly appear as shortened or dissolved along the cleavage surfaces (Figure 5a). As a consequence, dropstones have a general qualitative shape-preferred orientation subparallel to the cleavage seams (Figure 5a). Overall, the cleavage has all the characteristics of a pressure solution cleavage: (1) it is defined by dark, very fine grained seams; (2) cleavage intensity increases in what would be higher stress areas, such as areas where dropstones are near or in contact with each other (Figure 5b); (3) cleavage is more developed in finer grained material, i.e. the matrix, and not in coarse grained dropstones; (4) where the cleavage is in contact with dropstones, the dropstones are commonly cut off (inferred as dissolved) along the cleavage surface (Figure 5a-c); and (5) the cleavage is perpendicular to tensile fractures, as expected if dissolution cleavage and tensile fractured formed in the same stress field.

Composition of cleavage surfaces

X-Ray diffraction (XRD) and electron microprobe (EMP) analyses have been applied to address the composition of the fine-grained cleavage surfaces in the Dwyka diamictites. XRD was performed on powdered samples of matrix material, using a Phillips XRD system equipped with a PW 3830/40 generator, a PW 3710 MPD diffractometer control, and Xpert data collector and identity software, housed in the Department of Geological Sciences, University of Cape Town. Measurement conditions were 40 kV, 25 mA, CuK_{α} radiation with 1° slits, and samples were scanned from 3 to 70 °2θ with a step size of 0.025°2θ and counting time of 0.4 s. Element maps were measured using a JEOL JXA-8100 Electron Probe Microanalyser, housed in the Department of Geological Sciences, University of Cape Town. Analyses were performed with beam conditions of 15 kV, 18.5 nA, 12 ms dwell time, and spot size of 1 µm.

The XRD patterns are similar for all the exposed cycles of the Dwyka group in the field area (Figure 6). The peaks in the spectra can be accounted for by quartz, feldspar (albite ± anorthite and microcline), illite-muscovite, and chlorite. There may be a number of types of white mica here grouped and described as illite-muscovite, but detailed clay mineralogy is beyond the scope of this contribution. Based on relative intensity of XRD peaks, quartz is by far the most abundant mineral in the Dwyka matrix material, which is also apparent based on optical petrography (Fig. 5). Phyllosilicates are relatively minor, but present in all samples, and with chlorite appearing more abundant than white mica. There is no significant mineralogical difference between the matrix materials of the different Dwyka cycles, indicating that grain size is the only lithological parameter that varies significantly within the matrix of the Dwyka.

The element map in Figure 7 shows an area adjacent to a small, boudinaged, quartz clast. In this sample, clasts are elongate subparallel to cleavage surfaces. In an electron backscatter image, the cleavage planes appear relatively bright, compared to clasts of quartz. The edges of the quartz clasts are depleted in Si, in line with an interpretation of dissolution along grain boundaries. Quartz grain boundaries parallel to the cleavage are enriched in Fe and K, consistent with Fe-oxides and phyllosilicates. The cleavage seams have low Si concentrations, and show elevated concentrations of K, Al, and Fe, relative to the surrounding material. Ca is rare throughout the sample, and Ti was under the detection limit of the instrument (and therefore not displayed).

An area of high cleavage intensity was mapped and displayed in Fig. 8. Again, cleavage seams stand out in an electron backscatter image as brighter (greater number of backscattered electrons) than surrounding material. The seams are depleted in Si, marginally elevated in Al, and significantly enriched in K and Fe, compared to the rest of the sample. Feldspar (in the lower left corner) is partially replaced by K and minor Fe, consistent with hydration reactions locally forming phyllosilicates.

Discussion

Process and conditions of cleavage formation

The microstructure of the folded and cleaved Dwyka diamictites is typical of rocks deformed by pressure solution creep, with seams of insoluble material defining the cleavage planes. Specifically, the pressure solution cleavage in the Dwyka appears defined by phyllosilicates and Fe-oxides. Cleavage defined by dark, fine grained seams of Fe-oxides and phyllosilicates are also observed in other rocks inferred to have deformed by pressure solution creep, for example in the Otago Schist (Fagereng and Cooper, 2010), shales of the Shimanto Complex (Kawabata et al., 2007), along the San Andreas fault (Gratier *et al.*, 2011), and in the Willard thrust system, Utah (Yonkee et al., 2013). The pressure solution cleavage spacing is strongly affected by the size of competent dropstones within the Dwyka diamictites. On the outcrop scale, this leads to an anastomosing cleavage network separating less strongly cleaved lenses, appearing as ‘tombstones’ after weathering (Fig. 3a,b). The size of these less deformed lenses is a function of the dimensions of the largest dropstone each contains (Fig. 4). On the microscale, lithic, quartz and feldspar clasts in the matrix, which likely represent small dropstones, are not cleaved, and pressure solution cleavage wraps around the clasts (Fig. 5a-c). Cleavage intensity appears highest at clast boundaries and between closely spaced clasts (Fig. 5a,b), which are areas of inferred greater normal stress. This observation implies that cleavage seams developed preferentially in high stress areas, as expected for pressure solution cleavage (e.g. Durney, 1972).

Craddock *et al*. (2007) quantified the stress-strain field of cleavage formation in the Dwyka based on calcite twin fabric in syn-cleavage veins (subhorizontal calcite-filled extension fractures within clasts, as in Fig. 3c) and a limestone clast. They calculated a south-trending (181° average), subhorizontal least stretch, with a magnitude of – 4.8 %, in response to an average differential stress of 46 MPa. They also obtained a vertical intermediate strain axis, and an east-west trending, horizontal, greatest stretch. In the region where they took their samples and measurements, the folding in the Dwyka is approximately upright, with a subvertical cleavage (Fig. 2b), so that the least stretch is cleavage-normal and subhorizontal. Considering a larger area, cleavage is subvertical to moderately south-dipping (Fig. 2c), implying a subhorizontal to moderately northward-plunging least stretch. This is consistent with north-south shortening and pure shear in the Karoo Basin north of the Cape Fold Belt, and requires a component of top-to-the-north simple shear in the frontal range of the fold belt, consistent with northward movement of thrust sheets.

Consistent, subhorizontal, extension fracture orientations within dropstones (Craddock et al., 2007; this study), are consistent with a subvertical least compressive stress, as expected in an Andersonian stress field favouring reverse faulting. These extension fractures are confined to competent dropstones within the matrix, and their consistent orientation implies minor rotation of dropstones, at least around a horizontal axis, during deformation involving coeval folding, fracturing, and cleavage formation. The presence of subhorizontal tensile fractures, by itself, implies that at least locally and transiently, fluid pressure must have exceeded the lithostatic stress (Secor, 1965).

Kinetics of pressure solution creep

The importance of pressure solution in the development of the Cape Fold Belt depends on its kinetics; in other words whether it could achieve sufficiently high strain rates to be of significance to the overall deformation. Gratier *et al.* (2009) derived an empirical flow law for pressure solution creep limited by diffusion, of the form:

$$\dot{\varepsilon} = \frac{8DwcV_s\left(e^{3\Delta\sigma_n V_s / RT} - 1\right)}{d^3} \qquad (1)$$

where D is the diffusion constant along the stressed interface, w is the thickness of the fluid phase within which diffusion occurs, c is the solubility of the dissolved solid, V_s is the molar volume of the stressed solid, $\Delta\sigma_n$ is the driving stress, inferred to be the difference in normal stress between the stressed surface and a low stress deposition site (e.g. fluid pressure in a vein), R is the universal gas constant, T is temperature in Kelvin, and d is the diffusive mass transfer distance.

The parameter d is either fracture spacing or grain size. In this example, grain size is likely the control on mass transfer, as although veins are present locally within competent clasts, most mass transfer occurred by fluid-assisted grain boundary diffusion within the less competent matrix, as illustrated by cleavage development being characteristic of the matrix and not its clasts. If ‘tombstones’ are indeed defined by anastomosing cleavage planes, then the observation that tombstone size is controlled by drop stone size (Fig. 4), implies that grain size and cleavage spacing are related. This is not surprising, and implies that cleavage spacing is also a measure of *d*, as the transport distance from precipitation to dissolution is constrained by the distance to a dissolution seam.

Quartz is the main mineral dissolved along the dissolution seams, and is also a major component of the matrix (Figs. 6,7,8). The molar volume of quartz is 2.2×10^{-5} m^3 mol^{-1}. According to the empirical quartz solubility calculation of Rimstidt (1997), solubility of quartz in water at 200°C is approximately 4.3×10^{-3} mol m^{-3}, and goes up to 7.2×10^{-3} mol m^{-3} at 250°C (upper boundary of fluid temperature in the foothills of the Cape Fold Belt, Egle *et al*., 1998). The factors D and w are poorly constrained, but based on pressure solution experiments by Gratier *et al.* (2009) and quartz diffusion data presented by Brady (1995), D is approximately 1×10^{-10} m^2s^{-1} for the 200 - 350°C range, whereas w is between 2 and 10 nm (Gratier *et al.,* 2009). Like Gratier *et al*. (2009, 2011) I therefore use an average value for the product $Dw = 5.7 \times 10^{-19}$ m^3s^{-1}. A differential stress $\Delta\sigma_n$ of 46 MPa, measured by Craddock (2007) based on vein calcite is taken as an estimate for the stress difference between sites of dissolution and precipitation.

Figure 9 shows a plot of strain rate against *d*, contoured for temperature calculated using Eq. 1. The temperature control on quartz solubility does not have a major effect on strain rate compared to the potential variation in *d*. The factor *d* has a major effect arising both from inherent variation in diffusive distance in heterogeneous diamictites, and from the formulation of the pressure solution flow law (Eq. 1) where strain rate is inversely proportional to the cube of *d*. If cleavage spacing, typically between 10 μm and 1 mm (Fig 5), is representative of *d*, then for temperatures between 150 and 250°C, strain rates of 10^{-16} s^{-1} to 10^{-9} s^{-1} could be achieved. The range primarily represents a variation in transport distance between Dwyka cycles with high and low proportions of coarse dropstones. On the scale of orogenic strain rates, these potential strain rates achieved by pressure solution are high. For d less than about 0.3 mm, a grain size relatively common in the Dwyka matrix, as well as a distance comparable to cleavage spacing within this matrix (Fig. 5), predicted strain rate is higher than the global average of approximately 4×10^{-14} s^{-1} (Pfiffner and Ramsay, 1982), and higher than pressure solution strain rates of $1 - 4 \times 10^{-15}$ s^{-1} calculated for thrust sheets in the southern Pyrenees (Burbank et al., 1992; Holl and Anastasio, 1993), a fold-and-thrust belt deformed at comparable conditions to the Cape Fold Belt.

Implications for interpretations of the Cape Fold Belt

Discussion on strain distribution in the Cape Fold Belt (e.g. Paton et al., 2006), and interpretations on the relative contributions of faulting and folding (e.g. Booth and Shone, 2002; Booth, 2011), have not considered the contribution from cleavage development to overall horizontal shortening. The Dwyka diamictite is folded, but also contains a subvertical pressure solution cleavage contributing additional shortening. The magnitude of this shortening is unknown, and difficult to estimate. Based on dropstone shape change caused by pressure solution, one could qualitatively estimate shortening on the order of 5 % (Fig. 5), but this may underestimate shortening by dissolution of smaller inclusions and of the matrix material.

The strain rates associated with pressure solution are capable of similar or higher deformation rates to those typically associated with orogenic fold and thrust belts. Although the shortening associated with the Cape Fold Belt is poorly constrained, it should therefore be noted that pressure solution likely increases any current estimates. In addition, the potential strain rates accommodated by pressure solution creep imply that the viscosity of the Dwyka diamictites was sufficiently low for flow at strain rates typical of compressional margins. A corollary of this inference is that the Dwyka, despite containing large, strong clasts, had a bulk rheology that was relatively weak compared to surrounding quartzites (top of Cape Supergroup) and sandstones (higher in the Karoo Supergroup), which are highly fractured and thus their bulk rheology is better described by a Coulomb criterion with shear strength proportional to normal stress.

Cleavage formation and associated shape-preferred fabric in the Dwyka diamictites are interpreted to have formed by pressure solution creep, and little evidence is seen for soft sediment folding (although other soft sediment deformation, e.g. slumping, has been reported; Visser, 1997). Although pressure solution can occur at shallow depths, the diamictites were likely consolidated at the time the spaced axial planar cleavage developed. Consequently, folding would have initiated after at least some burial of the Dwyka Group, but at less than the 200-250°C inferred for the maximum temperature in this part of the Cape Fold Belt (Egle, 1998).

The axial planar cleavage in the Dwyka is consistent with pure shear, with a component of rotation around a horizontal axis present closer to the hinterland. This is typical for fold-and-thrust belts, and implies north-south shortening across the east-west trending southern arm of the Cape Fold Belt. This is consistent with uniaxial shortening, and does not require a transpressional component, as suggested by Tankard et al. (2009).

Conclusions

The Dwyka diamictite in the foreland of the Cape Fold Belt preserves an axial planar cleavage defined by very fine grained phyllosilicates and minor Fe-Mg oxides, interpreted as a spaced solution cleavage. The cleavage is anastomosing, with spacing controlled by the size of dropstones, which vary in the largest dimension from centimetres or less to more than a metre. Because the cleavage wraps around these dropstones, cleavage spacing and inferred strain intensity is highly variable, as reflected by the anastomosing nature of the cleavage.

Based on a pressure solution flow law, the strain rate that could be achieved by diffusive mass transfer in the Dwyka is sufficient to account for typical strain rates of 10^{-14} - 10^{-15} s^{-1} as inferred in other fold-and-thrust belts, or faster in finer grained Dwyka cycles. The potentially high strain rates imply that the Dwyka Group may have been a relatively weak layer within the folding sequence during formation of the Cape Fold Belt. Considering the dense cleavage spacing observed particularly in fine grained intervals, it is likely that the creation of a subvertical pressure solution cleavage contributed significantly to horizontal shortening in this area.

Acknowledgments

A UCT Research Development Grant and NRF Incentive Funding for Rated Researchers have provided funding for work on deformation mechanisms and deformation localization. I thank Carly Faber for assistance with fieldwork and development of the ideas presented in the manuscript, and I am grateful to Christel Tinguely and Tanya Dreyer for their efforts with the microprobe and XRD analyses. Two anonymous reviewers provided comments that improved the final paper.

References

Bangert, B., Stollhofen, H., Lorenz, V. and Armstrong, R. (1999). The Geochronology and significance of ash-fall tuffs in the glaciogenic Cerboniferous-Permian Dwyka Group of Namibia and South Africa. *Journal of African Earth Sciences*, **29**, 33-49.

Booth, P.W.K. (2011). Stratigraphic, structural and tectonic enigmas associated with the Cape Fold Belt: challenges for future research. *South African Journal of Geology*, **114**, 235-248.

Booth, P.W.K. and Shone, R.W. (2002). A review of thrust faulting in the Eastern Cape Fold Belt, South Africa, and the implications for current lithostratigraphic interpretation of the Cape Supergroup. *Journal of African Earth Sciences*, **34**, 179-190.

Brady, J.B. (1995). Diffusion data for silicate minerals, glasses, and liquids. *Mineral Physics and Crystallography: A Handbook of Physical Constants.* American Geophysical Union, Reference Shelf vol. 2, pp. 269-290.

Burbank, D.W., Verges, J., Muñoz, J.A. and Bentham, P. (1992). Coeval hindward- and forward-imbricating thrusting in the central southern Pyrenees, Spain: timing and rates of shortening and deposition. *Bulletin of the Geological Society of America*, **104**, 3-17.

Byerlee, J. D. (1978). Friction of rocks. *Pure and Applied Geophysics*, **116**, 615-626.

Catuneanu, O. (2004). Basement control on flexural profiles and the distribution of foreland facies: the Dwyka Group of the Karoo Basin, South Africa. *Geology*, **32**, 517-520.

Catuneanu, O., Hancox, P.J. and Rubidge, B.S. (1998). Reciprocal flexural behaviour and contrasting stratigraphies: a new basin development model for the Karoo retroarc foreland system, South Africa. *Basin Research*, **10**, 417-439.

Catuneanu, O., Wopfner, H., Eriksson, P.G., Cairncross, B., Rubidge, B.S., Smith, R.M.H. and Hancox, P.J. (2005). The Karoo basins of south-central Africa. *Journal of African Earth Sciences*, **43**, 211-253.

Craddock, J.P., McKiernan, A.W. and de Wit, M.J. (2007). Calcite twin analysis in syntectonic calcite, Cape Fold Belt, South Africa: Implications for fold and cleavage formation within a shallow thrust front. *Journal of Structural Geology*, **29**, 1100-1113.

Dalziel, I.W.D., Lawver, L.A. and Murphy, J.B. (2000). Plumes, orogenesis, and supercontinental fragmentation. *Earth and Planetary Science Letters*, **178**, 1-11.

de Wit, M.J. and Ransome, I.G.D. (1992). Regional inversion tectonics along the southern margin of Gondwana. *In* M.J. de Wit and I.G.D. Ransome (Editors), Inversion Tectonics of the Cape Fold Belt, Karoo and Cretaceous Basins of Southern Africa. Balkema, Rotterdam, pp. 15-22.

Durney, D. W. (1972). Solution-transfer, an important geological deformation mechanism. *Nature,* **235**, 315-317.

du Toit, A.L. (1937). *Our Wandering Continents*. Oliver and Boyd, Edinburgh.

Egle, S., de Wit, M.J. and Hoernes, S. (1998). Gondwana fluids and subsurface palaeohydrology of the Cape Fold Belt and the Karoo Basin, South Africa. *Journal of African Earth Sciences*, **27**, 63-64.

Fagereng, Å. (2012). A note on folding mechanisms in the Cape Fold Belt, South Africa. *South African Journal of Geology*, **115**, 137-144.

Fagereng, Å. and Cooper, A.F. (2010). The metamorphic history of rocks buried, accreted and exhumed in an accretionary prism: an example from the Otago Schist, New Zealand. *Journal of Metamorphic Geology*, **28**, 935-954.

Gratier, J.P. and Gamond, J.F. (1990). Transition between seismic and aseismic deformation in the upper crust. *In* R.J. Knipe and E.H. Rutter (Editors), Deformation Mechanisms, Rheology and Tectonics. Geological Society, London, *Special Publication*, **54**, 461-473.

Gratier, J.P., Guiguet, R., Renard, F., Jenatton, L. and Bernard, D. (2009). A pressure solution creep law for quartz from indentation experiments. *Journal of Geophysical Research-Solid Earth*, **114**, doi:10.1029/2008JB005652.

Gratier, J.P., Richard, J., Renard, F., Mittempergher, S., Doan, M.-L., Di Toro, G., Hadizadeh, J. and Boullier, A.-M. (2011). Aseismic sliding of active faults by pressure solution creep: Evidence from the San Andreas Fault Observatory at Depth. *Geology*, **39**, 1131-1134.

Gratier, J.P., Dysthe, D. and Renard, F. (2013). The role of pressure solution creep in the ductility of the Earth's upper crust. *Advances in Geophysics*, **54**, doi:10.1016/B978-0-12-380940-7.00002-0.

Hälbich, I.W., 1992. The Cape Fold Belt orogeny: State of the art 1970s-1980s. *In* M.J. de Wit and I.G.D. Ransome (Editors), Inversion Tectonics of the Cape Fold Belt, Karoo and Cretaceous Basins of Southern Africa. Balkema, Rotterdam, pp. 141-158.

Hälbich, I.W.,1993. The Cape Fold Belt-Agulhas Bank transect across Gondwana Suture, Southern Africa. *Global Geoscience Transect*, **9**, American Geophysical Union, Washington, 18 pp.

Holl, J.E., Anastasio, D.J., 1993. Paleomagnetically derived folding rates southern Pyrenees, Spain. *Geology*, **21**, 271-274.

Kawabata, K., Tanaka, H., Kimura, G., 2007. Mass transfer and pressure solution in deformed shale of accretionary complex: Examples from the Shimanto Belt, southwestern Japan. *Journal of Structural Geology*, **29**, 697-711.

Kohlstedt, D. L., Evans, B., Mackwell, S. J., 1995. Strength of the lithosphere: constraints imposed by laboratory experiments. *Journal of Geophysical Research-Solid Earth*, **100**, 17587-17602.

Lindeque, A., de Wit, M.J., Ryberg, T., Weber, M., Chevallier, L., 2011. Deep crustal profile across the southern Karoo basin and Beattie magnetic anomaly, South Africa: an integrated interpretation with tectonic implications. *South African Journal of Geology*, **114**, 265-292.

Lock, B.E., 1980. Flat-plate subduction and the Cape Fold Belt of South Africa. *Geology*, **8**, 35-39.

Mantero, E.M., Alonso-Chaves, F.M., Carcia-Navarro, E., Azor, A., 2011. Tectonic style and structural analysis of the Puebla de Guzman Antiform (Iberian Pyrite Belt, South Portuguese Zone, SW Spain). *In* J. Poblet and R.J. Lisle (Eds.), *Kinematic Evolution and Structural Styles of Fold-and-Thrust Belts*. Geological Society, London, *Special Publication*, **349**, 199-218.

McClay, K.R., 1977. Pressure solution and Coble creep in rocks and minerals. *Journal of the Geological Society*, **134**, 57-70.

Mitra, S., 1990. Fault-propagation folds: geometry, kinematics and hydrocarbon traps. *AAPG Bulletin*, **74**, 921-945.

Paton, D.A., 2006. Influence of crustal heterogeneity on normal fault dimensions and evolution: southern South Africa extensional system. *Journal of Structural Geology*, **28**, 868-886.

Paton, D.A., Macdonald, D.I.M., Underhill, J.R., 2006. Applicability of thin or thick skinned structural models in a region of multiple inversion episodes; southern South Africa. *Journal of Structural Geology*, **28**, 1933-1947.

Pfiffner, O.A., Ramsay, J.G., 1982. Constraints on geological strain rates: arguments from finite strain states of naturally deformed rocks. *Journal of Geophysical Research*, **87**, 311-321.

Rimstidt, J.D., 1997. Quartz solubility at low temperatures. *Geochimica et Cosmochimica Acta*, **13**, 2553-2558.

Rutter, E. H., 1983. Pressure solution in nature, theory and experiment. *Journal of the Geological Society of London*, **140**, 725-740.

Secor, D.T., 1965. Role of fluid pressure in jointing. *American Journal of Science*, **263**, 633-646.

Sibson, R.H., 1983. Continental fault structure and the shallow earthquake source. *Journal of the Geological Society*, **140**, 741-767.

Suppe, J., 1983. Geometry and kinematics of fault-bend folding. *American Journal of Science*, **283**, 684-721.

Tankard, A., Welsink, H., Aukes, P., Newton, R., Stettler, E., 2009. Tectonic evolution of the Cape and Karoo basins of South Africa. *Marine and Petroleum Geology,* **26**, 1379-1412.

Visser, J.N.J., 1987. The influence of topography on the Permo-Carboniferous glaciation in the Karoo Basin and adjoining areas, Southern Africa. *In* D.H. Elliot, J.W. Collison, G.D. McKenzie and S.M. Haban (Editors), *Gondwana 6*, American Geophysical Union, Washington, pp. 123-129.

Visser, J.N.J., 1997. Deglaciation sequences in the Permo-Carboniferous Karoo and Kalahari basins of southern Africa: A tool in the analysis of cyclic glaciomarine basin fills. *Sedimentology*, **44**, 507-521.

Visser, J.N.J., van Niekerk, B.N.,van der Merwe, S.W., 1997. Sediment transport of the Late Paleozoic glacial Dwyka Group in the southwestern Karoo Basin. *South African Journal of Geology*, **100**, 223-236.

Yonkee, W.A, Czech, D.M., Nachbor, A.C., Barszewski, C., Pantone, S., Balgord, E.A., Johnson, K.R., 2013. Strain accumulation and fluid-rock interaction in a naturally deformed diamictites, Willard thrust system, Utah (USA): Implications for crustal rheology and strain softening. *Journal of Structural Geology*, **50**, 91-118.

Figure captions

Figure 1: a) Map showing simplified lithostratigraphy of the Cape Fold Belt and the location of the study area near Laingsburg (after Paton *et al.*, 2006; Tankard *et al.*, 2009). The dashed line shows the location of the Cape Fold Belt-Agulhas Bank Transect (Hälbich, 1993), on which the cross-section in (b) is based. b) Cross-section illustrating the north-south variation in geometry across the Cape Fold Belt (after Hälbich, 1993; Paton, 2006). The study area is along strike from the northern end of this cross section, where the base of the Karoo Supergroup crops out, and folding style changes from inclined to upright. c) Simplified cross-section of the study area, illustrating the change in folding style from south to north.

Figure 2: Lower hemisphere, equal area stereoplots showing representative, regional fold limbs (solid great circles) and axial planes (dashed great circle) in the (a) southern and (b) northern parts of the study area. Note the change from moderately inclined to upright folding from south to north, over a distance of approximately 10 km (c.f. Fig. 1c). (c) Poles to planes for cleavage in

Dwyka diamictite in the south (open circles) and north (filled circles), with dashed great circles representing the average cleavage planes in the south and north of the study area. Note the approximately axial planar orientation of the cleavage planes.

Figure 3: Field photographs of Dwyka diamictite. (a) Rare exposure of bedding in the Dwyka Group (cycle 2c), defined by a subvertical boulder bed. The average plane of the anastomosing cleavage dips about 45° to the south. (b) Well developed 'tombstone' cleavage in Dwyka (cycle 3c), further north than (a), and the cleavage is here steeply inclined. (c) Close up on subvertical cleavage in Dwyka cycle 3c, where subhorizontal fractures (perpendicular to cleavage) can be seen within a dropstone.

Figure 4: Logarithmic plot of longest dimension of largest contained dropstone against 'tombstone' long axis length. The plot illustrates the qualitative observation that the size of 'tombstones' of Dwyka, defined by preferential weathering along cleavage planes, is controlled by the size of dropstones within the 'tombstones'. This emphasizes that cleavage spacing is controlled by dropstone size.

Figure 5: Photomicrographs in plane polarized light of cleavage seams in Dwyka Group diamictites (all cycle 3c) cut perpendicular to cleavage. All the photographs are rotated such that the average cleavage orientation is subhorizontal. (a) Relatively distributed cleavage, note dissolved edges of quartz clasts (arrows), and the anastomosing nature of the, on average, horizontal cleavage in this photomicrograph. (b) High cleavage density at the edge, and between edges, of larger dropstones, again note the dissolved edges of quartz clasts (white arrows). (c)

Sealed tensile microfractures within a small dropstone. Note that the fractures are perpendicular to cleavage in surrounding matrix (white arrows), indicating the fractures and cleavage formed in the same stress field.

Figure 6: X-ray diffraction spectra of matrix material from a representative sample from each cycle of the Dwyka diamictite exposed in the study area. Little variation is observed between the different cycles, and the major minerals are quartz, feldspars (albite, anorthite, and microcline), illite-muscovite, and chlorite, in all samples.

Figure 7: Electron backscatter (EBS) image and element maps of the area indicated by the white rectangle on the photomicrograph (plane polarized light). On the element maps, warm colours (red, yellow) represent high relative abundance, and cold colours (blue, black) relatively low abundance. Cleavage seams stand out as bright on the EBS image, and are depleted in Si, enriched in Al, K, and Fe. Scale bars are 100 μm long.

Figure 8: Electron backscatter (EBS) image and element maps of the area indicated by the white rectangle on the photomicrograph (plane polarized light), an area of particularly dense solution cleavage. On the element maps, warm colours (red, yellow) represent high relative abundance, and cold colours (blue, black) relatively low abundance. Cleavage stands out as bright on the EBS image, and is depleted in Si, enriched in Al, K, and Fe. Scale bars are 50 μm long.

Figure 9: Plot of strain rate (base 10 logarithm) against diffusive distance *d* calculated for a pressure solution flow law assuming diffusion as the rate-limiting process (Gratier et al., 2009).

The plot is contoured for temperature, and a shaded area shows typical cleavage spacing (and grain size) in the Dwyka Group diamictite.

Figure 1

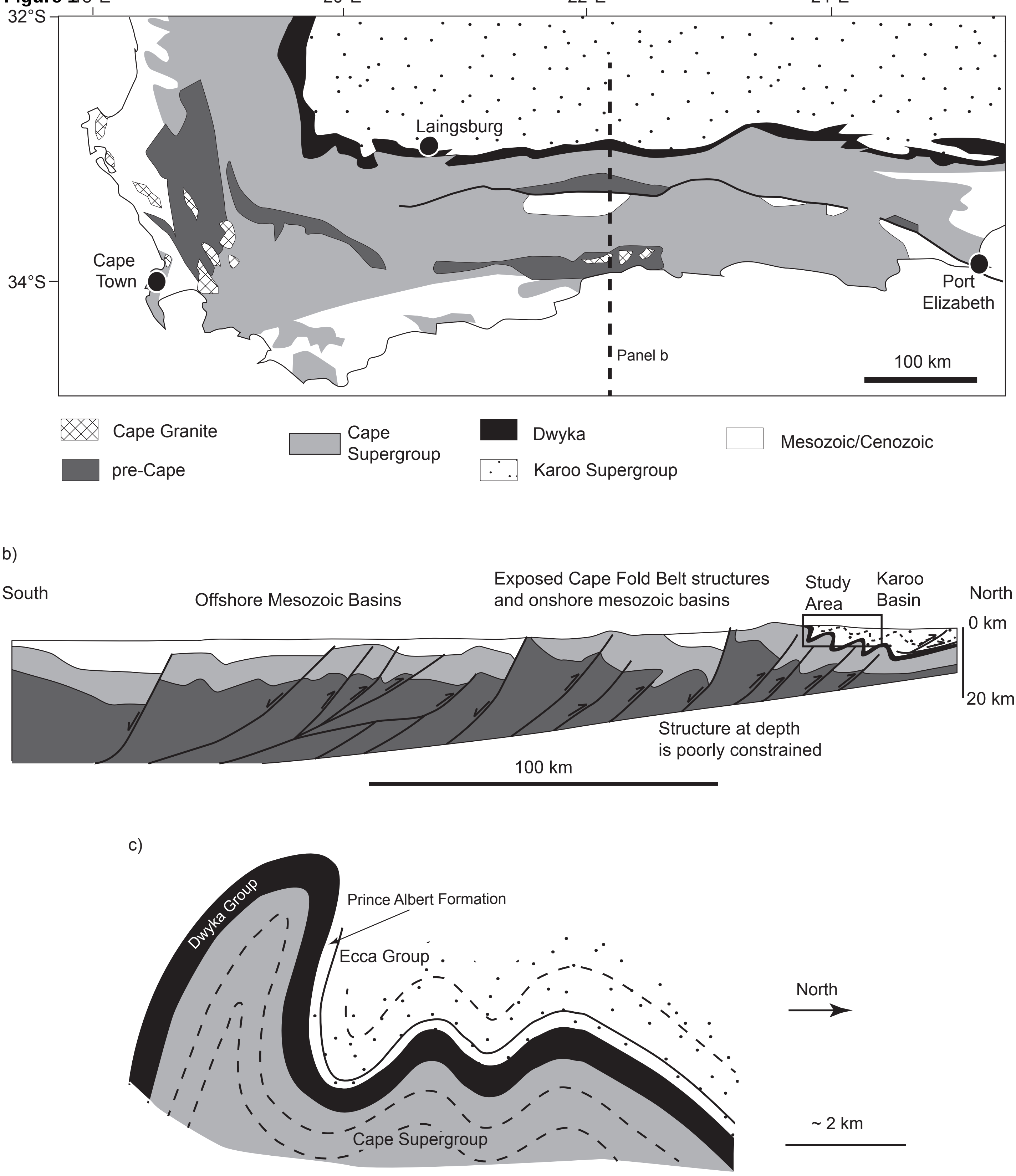
a)
18°E
20°E
22°E
24°E
32°S
34°S
Laingsburg
Cape
Town
Port
Elizabeth
Panel b
100 km
Cape Granite
pre-Cape
Cape
Supergroup
Dwyka
Karoo Supergroup
Mesozoic/Cenozoic
b)
South
Offshore Mesozoic Basins
Exposed Cape Fold Belt structures
and onshore mesozoic basins
Study
Area
Karoo
Basin
North
0 km
20 km
Structure at depth
is poorly constrained
100 km
c)
Dwyka Group
Prince Albert Formation
Ecca Group
North
~ 2 km
Cape Supergroup

Figure 2

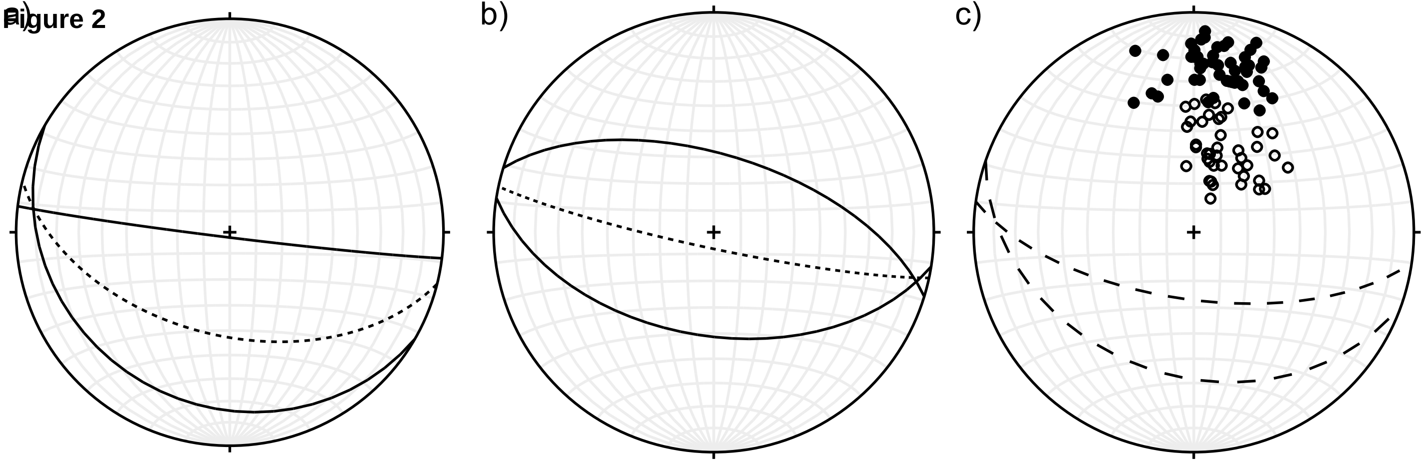

Figure 3

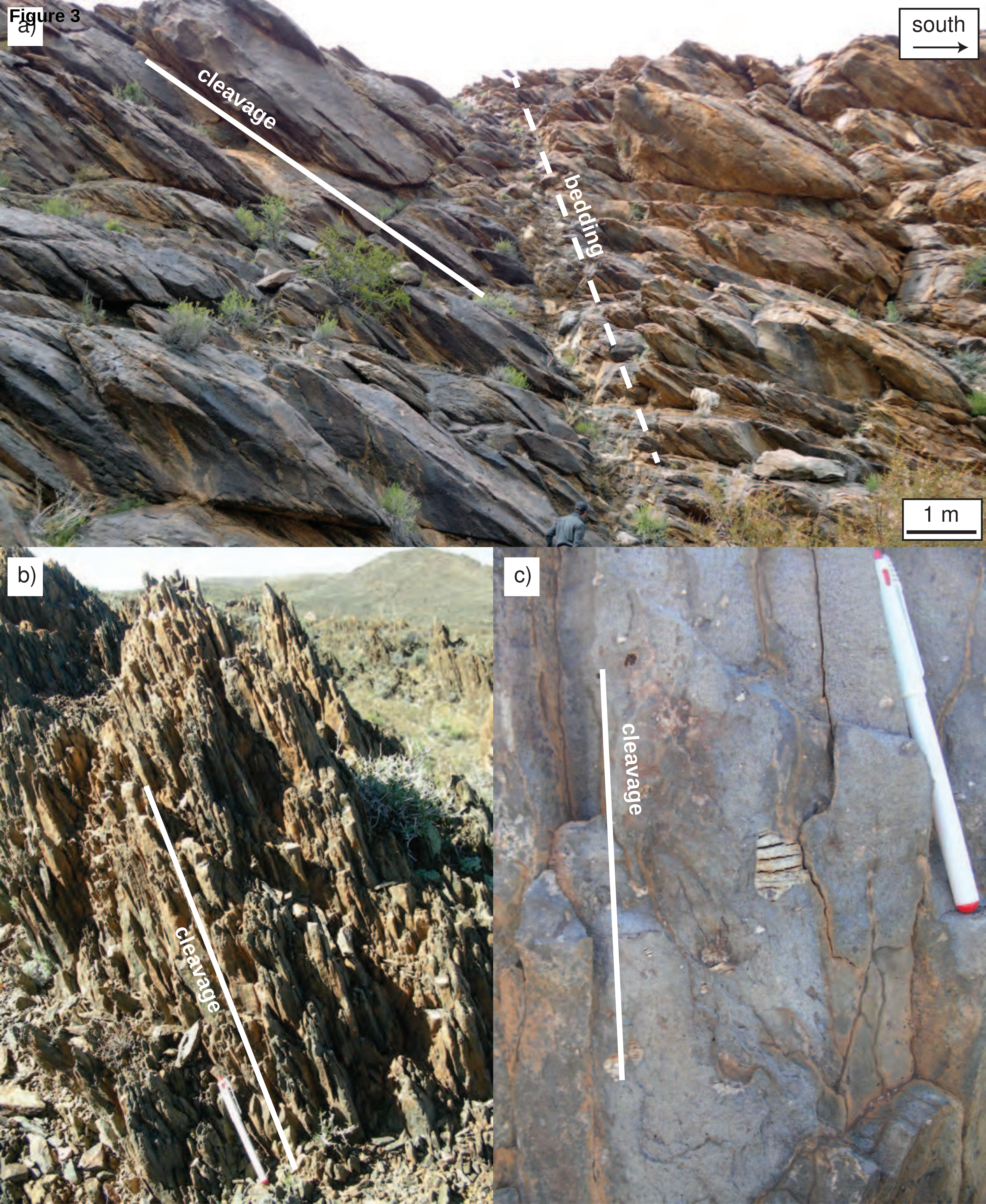

Figure 4

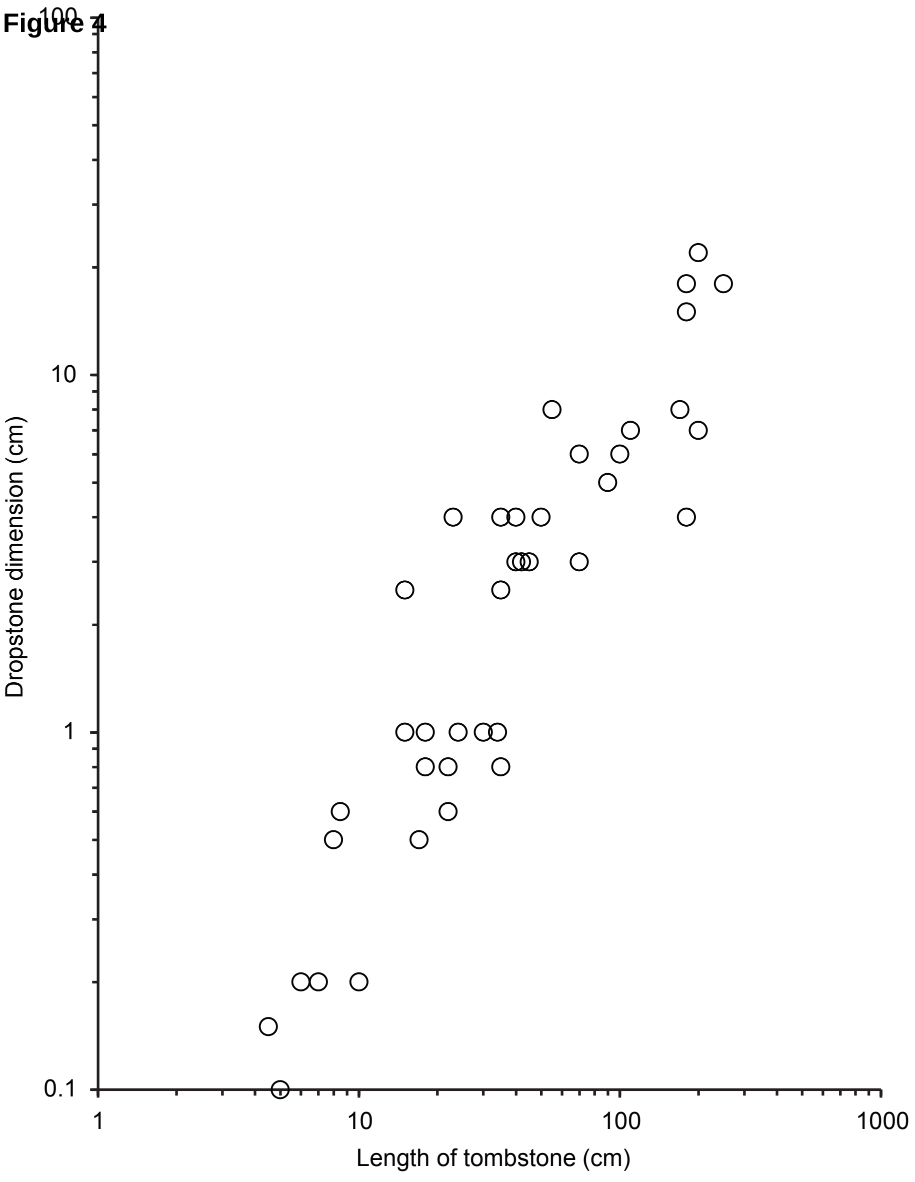
100
10
1
0.1
Dropstone dimension (cm)
1
10
100
1000
Length of tombstone (cm)

Figure 5

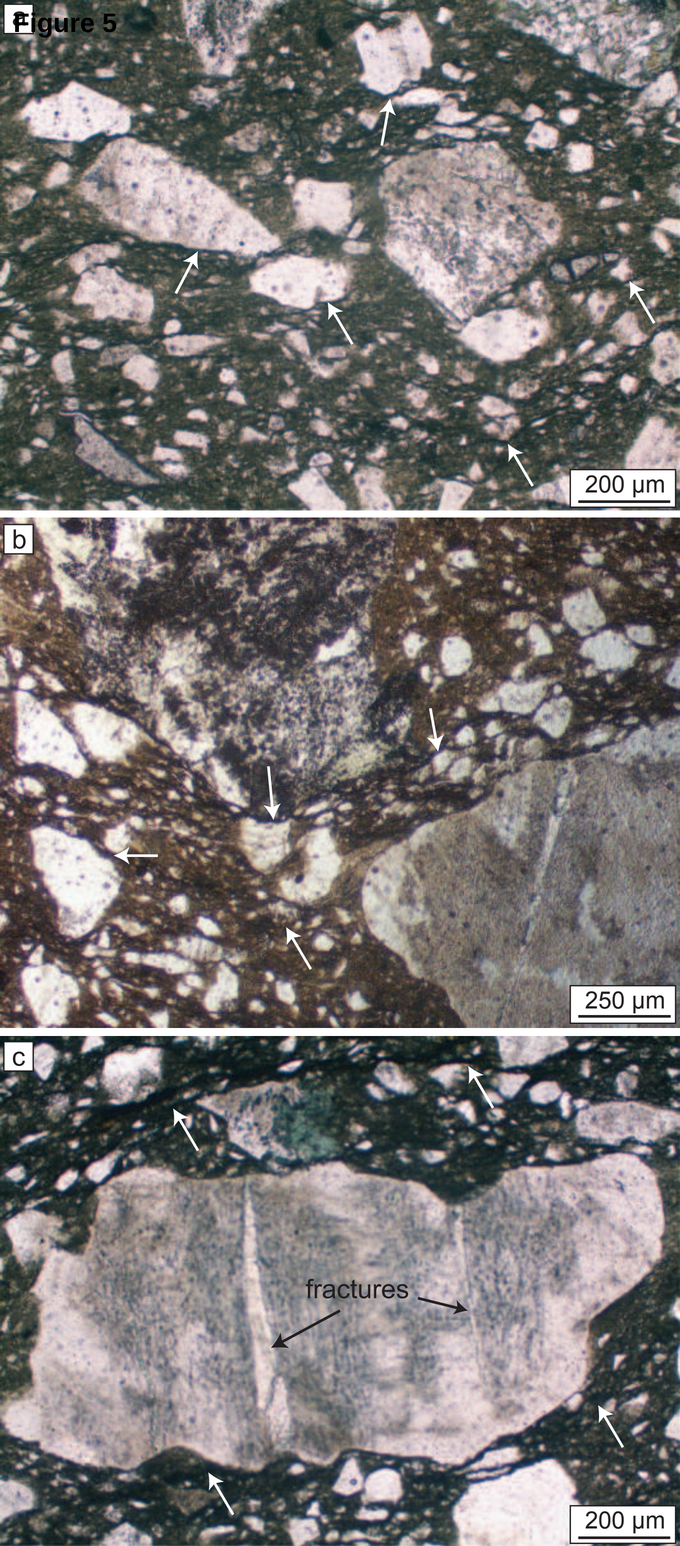

Figure 6

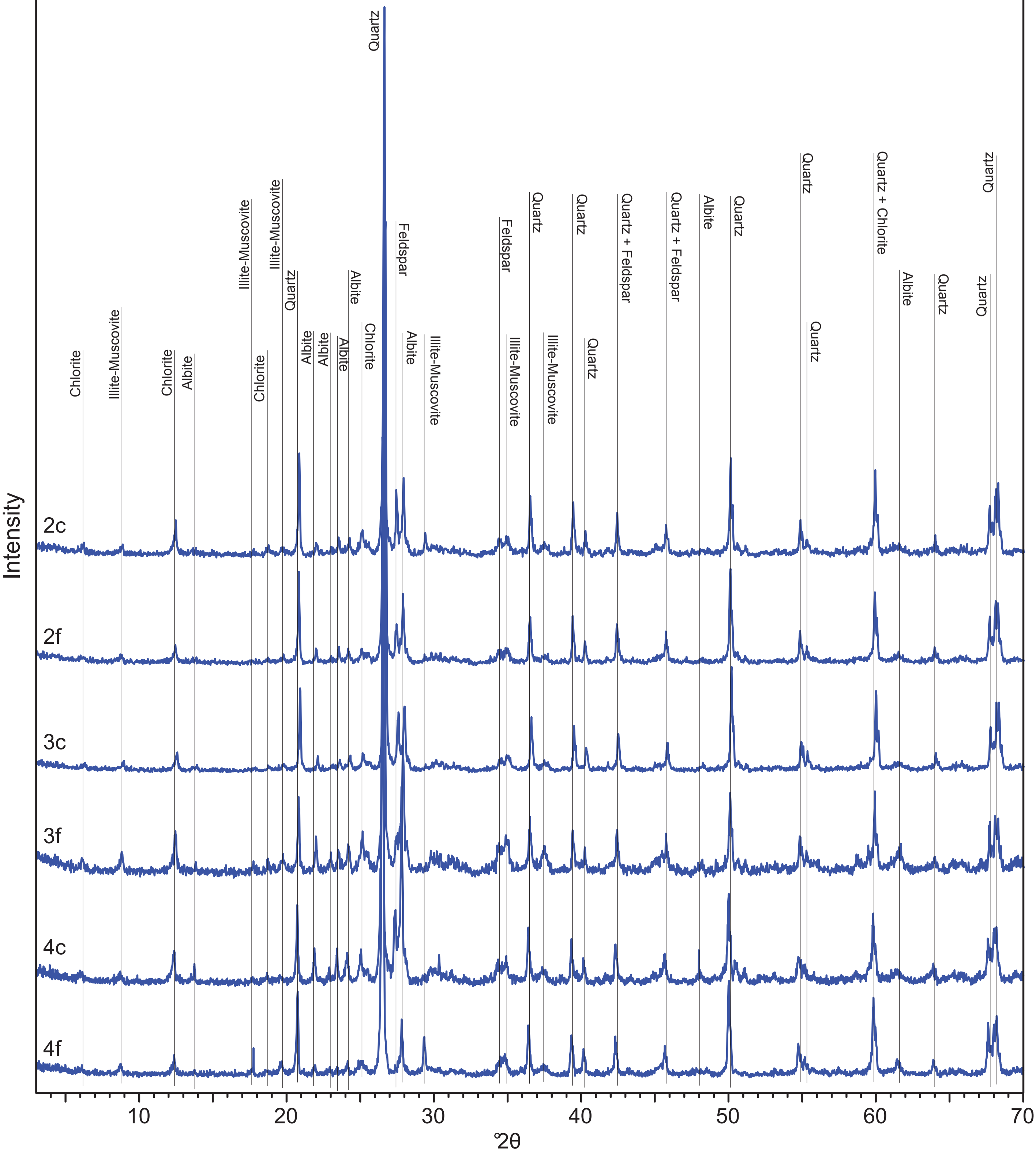
Quartz
Chlorite
Illite-Muscovite
Chlorite
Albite
Illite-Muscovite
Chlorite
Illite-Muscovite
Quartz
Albite
Albite
Albite
Albite
Chlorite
Feldspar
Albite
Illite-Muscovite
Feldspar
Illite-Muscovite
Quartz
Illite-Muscovite
Quartz
Quartz
Quartz + Feldspar
Quartz + Feldspar
Albite
Quartz
Quartz
Quartz
Quartz + Chlorite
Albite
Quartz
Quartz
Quartz
2c
2f
3c
3f
4c
4f
Intensity
10
20
30
40
50
60
70
°2θ

Figure 7

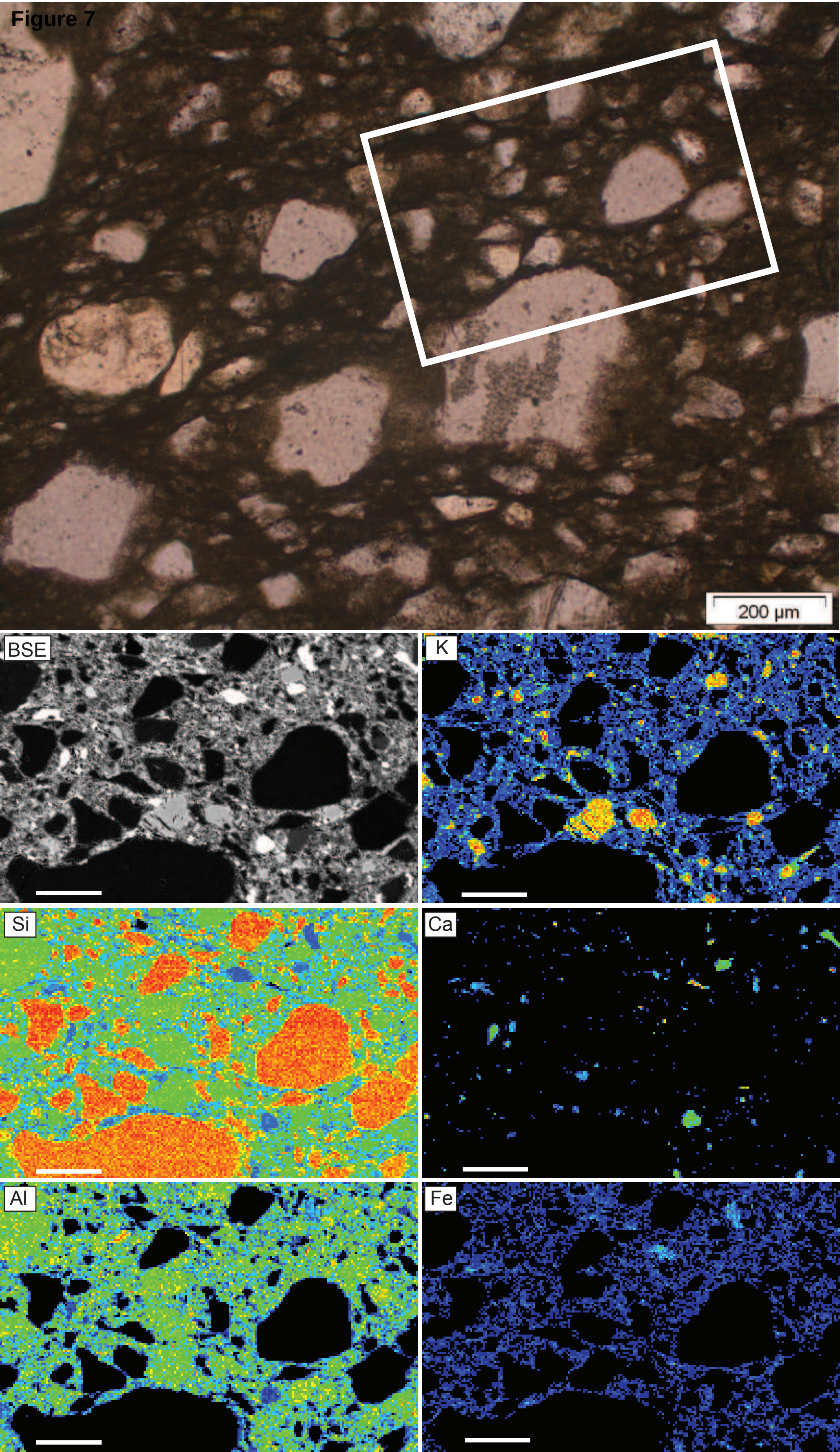

Figure 8